Journal of Materials Chemistry A

PAPER

View Article Online
View Journal | View Issue

Cite this: J. Mater. Chem. A, 2015, 3, 20305

Thiophene-modified perylenediimide as hole transporting material in hybrid lead bromide perovskite solar cells†

Jaykrushna Das,‡[a] Raja Bhaskar Kanth Siram,‡[b] David Cahen,[a] Boris Rybtchinski*[b] and Gary Hodes*[a]

Received 29th June 2015
Accepted 25th August 2015

DOI: 10.1039/c5ta04828a

www.rsc.org/MaterialsA

A small molecule based on *N*,*N*′-dialkyl perylenediimide (PDI) as core derivatized with thiophene moieties (Th-PDI) was synthesized. Its HOMO (highest occupied molecular orbital) level was measured to be between 5.7 and 6.3 eV *vs.* local vacuum level depending on doping and measurement method. Th-PDI was successfully applied as hole-transporting material (HTM) in $CH_3NH_3PbBr_3$ hybrid perovskite solar cells. Three different cell architectures, each with a different mode of operation, were tested: (1) using a mesoporous (mp) TiO_2 substrate; (2) mp-Al_2O_3 substrate; (3) planar dense TiO_2 substrate. The first gave the best overall efficiency of 5.6% while the mp-Al_2O_3 gave higher open-circuit photovoltage (V_{OC}) but lower efficiency (2.2%). The cells exhibited good reproducibility with very little *J*–*V* hysteresis (the mp-Al_2O_3 showed a more appreciable hysteresis of individual photovoltaic parameters but little dependence of efficiency on scan direction). Storage of unencapsulated cells in 25–30% relative humidity demonstrated fairly good stability with <20% efficiency drop after 37 days. While further optimization of each layer in the device is needed, the synthetically-simple new molecule shows promise as an inexpensive and readily-doped HTM for use in photovoltaic cells where a deep HOMO level is needed.

Introduction

Organic–inorganic lead halide perovskites have shown great potential for application in solar cells.[1–6] They exhibit many favorable properties, including a steep absorption onset with strong light absorption, high carrier mobility and long carrier lifetimes. The two latter properties result in very long charge diffusion lengths.[7,8] Another feature of these cells is the relatively high open-circuit voltage (V_{OC}) with values up to 1.15 V (ref. 9) reported for $CH_3NH_3PbI_3$ ($E_g \sim 1.6$ eV) and 1.5 V (refs. 10 and 15) for the corresponding bromide ($E_g \sim 2.3$ eV). High V_{OC} solar cells are of great interest as they could be utilized as the top cell in tandem devices, in other spectrally split cells or for driving electrochemical reactions.[11]

To obtain high voltages from the higher band gap $CH_3NH_3PbBr_3$ (abbreviated to $MAPbBr_3$), a hole transporting material (HTM) that is reasonably well-matched with the perovskite valence band is necessary. The first high voltage cell of this type, with $V_{OC} = 1.3$ V, was made using *N*,*N*′-dialkyl perylenediimide (PDI) with a low-lying highest occupied molecular orbital (HOMO) level.[12] Following this a V_{OC} of 1.5 V was achieved using 4,4′-bis(*N*-carbazolyl)-1,1′-biphenyl (CBP) as an HTM having a lower-lying HOMO level.[10] In both cases the efficiency of the cell was low or modest. Subsequently higher efficiency cells have been reported at (in order of publication date) 6.7%,[13] 5.4%,[14] 10.4% (ref. 15) and 8.7% (ref. 16) with varying values of V_{OC}. The HTMs used in these cells were poly(triarylamine) (PTAA) polymer and its derivatives,[13,15] CBP[14] and spiro OMeTAD.[16] With the exception of PDI, these HTMs are relatively expensive due to the extensive and tedious synthetic processes required for their preparation.

In view of the lack of inexpensive, easy-to-make HTMs with low-lying HOMO levels, as well as in order to expand the choice of such HTMs in general, we have looked for suitable alternatives. In this paper, we report on a novel PDI derivative made by a simple synthesis with high yield that was successfully applied as an HTM in $MAPbBr_3$ perovskite solar cells. PDI-based molecules typically have a HOMO level of ≥6 eV,[17] an attractive feature for high V_{OC}. In our earlier report using PDI, in spite of the 1.3 V V_{OC}, we obtained a low efficiency of 0.56% with 1 mA cm^{-2} short circuit current density (J_{SC}).[12] We attributed this, at least in part, to the high resistance of the PDI. It has been reported in the literature that the conductivity of PDI can be increased by incorporating electron donating groups.[18,19] Since thiophene is a good electron donating group[20] (DFT calculations

[a]Department of Materials and Interfaces, Weizmann Institute of Science, Rehovot 7610001, Israel. E-mail: gary.hodes@weizmann.ac.il

[b]Department of Organic Chemistry, Weizmann Institute of Science, Rehovot 7610001, Israel. E-mail: boris.rybtchinski@weizmann.ac.il

† Electronic supplementary information (ESI) available. See DOI: 10.1039/c5ta04828a

‡ JD and RBKS contributed equally.

show this behavior in the form of electron density diagrams in Fig. S1†), we attached a thiophene heterocycle at the bay position of PDI to explore the resulting system as a HTM in perovskite solar cells Additionally, for better solubility of this PDI in common organic solvents, *n*-hexyl chains were attached to the thiophene ring.

Results and discussion

The targeted thiophene modified PDI, *N*,*N*′-bis(ethylpropyl)-1,7-bis(5-*n*-hexyl-2-thienyl)perylene-3,4,9,10-diimide (abbreviated as Th-PDI) was synthesized as outlined in Scheme 1. The detailed synthetic procedure can be found in the experimental section of the (ESI†). The molecule has good solubility in all common organic solvents, which enables easy solution-processable fabrication of devices by spin-coating. Doping was carried out using lithium bis(trifluoromethanesulfonyl)imide (Li-$[CF_3SO_2]_2$N-LiTFSI) and 4-*tert*-butylpyridine (*t*BP).

In contrast to PDI which has been shown to be crystalline,[21] the Th-PDI showed only very broad background peaks in XRD, typical of amorphous material.

The absorption and emission spectra of (undoped) Th-PDI, both in solution (in chloroform) and as a spin-coated thin film are presented in Fig. 1a. The energy gap between the HOMO and the lowest unoccupied molecular orbital (HOMO–LUMO gap) was estimated from the onset of the absorption spectrum as 1.8 eV. The energy levels of the HOMO and the lowest unoccupied molecular orbital (LUMO) were determined from the onset of the first Th-PDI oxidation and reduction potentials respectively, measured by cyclic voltammetry (CV, Fig. 1b) and give a HOMO–LUMO gap in good agreement with the optical spectra. The potentials of the HOMO and LUMO levels on the solid state scale were calculated from the following equations:[22,23]

$$\mathrm{HOMO} = E^{\mathrm{ox}}_{\mathrm{onset}} + 4.7\ \mathrm{eV}$$

$$\mathrm{LUMO} = E^{\mathrm{red}}_{\mathrm{onset}} + 4.7\ \mathrm{eV}$$

Ultraviolet photoelectron spectroscopy (UPS) was also used to independently probe the HOMO level position and determine the work function (WF) of the material. The HOMO energy levels were found to be 6.1 eV and 6.3 eV for undoped and doped Th-PDI, respectively. To a first approximation, the HOMO and LUMO levels do not change upon doping and the change we measure may be due to change/formation of an interfacial dipole at the HTM surface. All the results obtained from absorption, emission and CV measurements are summarized in Table 1.

The work functions were also measured by Kelvin probe (KP) and found to be 5.0 and 5.2 eV for the undoped and doped material respectively. The WFs and HOMO levels measured by CV, UPS and KP are given in Table 2. The 0.4 V difference between the electrochemical and UPS measurements of the (undoped) Th-PDI HOMO position is not too surprising considering the limitations of the methods and averaging the two methods gives a value of 5.9 ± 0.2 eV. As noted above, doping shifts this further downwards by ~0.2 eV. The WFs also shift to higher values on doping as expected, although less than might be anticipated.

The $MAPbBr_3$ films were made using MABr and $PbCl_2$ (see ESI† for details) to improve the film morphology.[10] However, both the optical spectrum and the XRD pattern were identical with the pure bromide perovskite and we were unable to detect any chlorine content by energy dispersive spectroscopy (EDS) measurements. XPS analysis showed traces of Cl (~1–2.5% relative to Br). This suggests the presence of small amounts of Cl at the surface since it is not matched by the EDS. We therefore designate the material as $MAPbBr_3$ rather than as a solid solution with Cl.

Plan view scanning electron microscopy (SEM) images were taken to analyze the coverage and morphology on different substrates used in this work (Fig. S2,† and discussed there; see also below). In brief, deposition on mp-TiO_2 gives rise to a smaller crystal size and substantially better coverage compared to the other two substrates (dense TiO_2 and mp-Al_2O_3).

Photovoltaic cell measurements

We used the new PDI-derivative, Th-PDI, as a HTM in $MAPbBr_3$-based solar cells with three different cell architectures: (a)

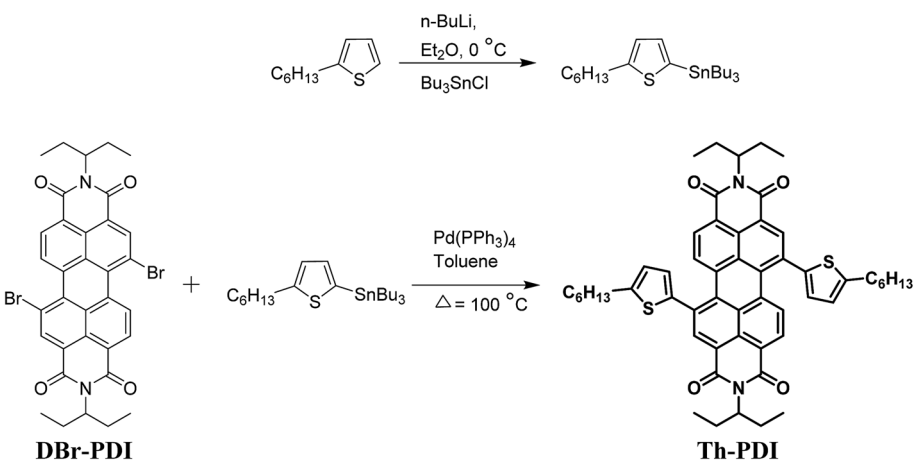

Scheme 1 Schematic diagram describing the synthesis of Th-PDI.

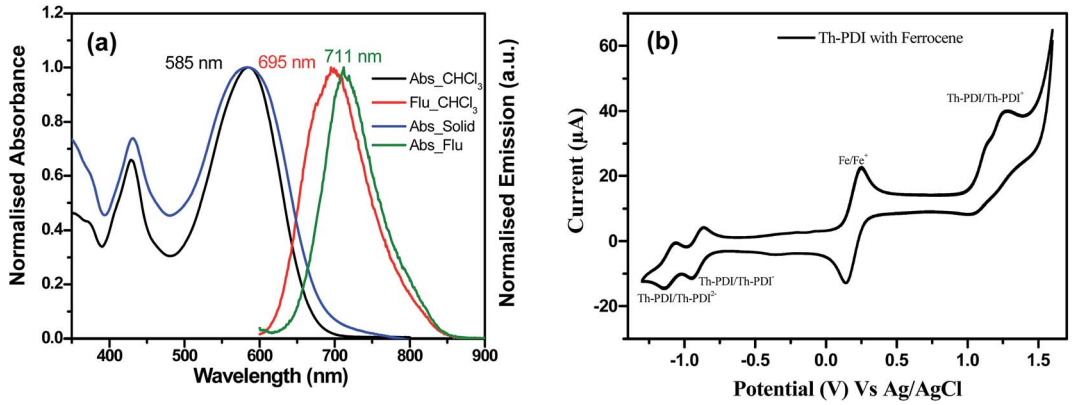

Fig. 1 (a) UV-Vis absorption and corresponding emission spectra of Th-PDI in chloroform solution and as a spin-coated thin-film on quartz (thickness ~ 100 nm). (b) Cyclic voltammogram of Th-PDI in dichloromethane with tetrabutyl ammonium hexafluorophosphate (Bu_4NPF_6) as supporting electrolyte and ferrocene as an internal standard. The Th-PDI was undoped.

planar heterojunction solar cell without any mesoporous oxide layer *i.e.*, flat cell structure (dense TiO_2); (b) on mesoporous TiO_2 (mp-TiO_2); and (c) meso-superstructured solar cell (MSSC) where mesoporous Al_2O_3 (mp-Al_2O_3) was used instead of TiO_2 and which is presumed to be electronically inert and simply acts as a scaffold for the perovskite absorber.

Fig. 2 shows a cross-sectional SEM image of a complete cell using mp-TiO_2 (the SEM images for the planar and mp-Al_2O_3 substrates are shown in Fig. S3†). The image shows ~500 nm thick perovskite capping layer, in addition to the infiltration of perovskite into the mesoporous oxide layer. From the corresponding backscattered image (Fig. 2b), it is evident that the perovskite capping layer is rather heterogeneous. More work is underway to obtain continuous and smooth perovskite films, which should give better cells (although such films may block the HTM infiltration into the mp-TiO_2/perovskite structure).

A schematic energy level alignment of the different components of the cell with the HOMO level of doped Th-PDI (determined by UPS) used in this work is also included, as Fig. 2c.

Considering the mesoporous TiO_2 cells, made with the as-prepared (undoped) HTM, under standard AM 1.5 solar light of 100 mW cm^{-2} intensity (Fig. 3A, plot a), a short-circuit photocurrent (J_{SC}) of 5.7 mA cm^{-2}, an open-circuit photovoltage (V_{OC}) of 1.09 V and fill factor (FF) of 0.52 were obtained, with an overall light-to-electric power conversion efficiency (PCE) of 3.3%. When the HTM was doped with 4-*tert*-butylpyridine (*t*BP) and Li-$[CF_3SO_2]_2$N-LiTFSI, all the parameters improved dramatically with J_{SC} = 7.6 mA cm^{-2}, V_{OC} = 1.23 V, FF = 0.6 and PCE = 5.6% for the best cell (plot b in Fig. 4A). This increase can be attributed in part to the improvement of HTM conductivity. This improvement is evidenced by the strong reduction in series resistance of the doped cell compared to the equivalent undoped cell that can be seen from the high forward bias region of the dark *J–V* curves in Fig. 3A and, with better clarity, in Fig. S4.† As reported in the literature, LiTFSI is a p-type dopant in other organic hole conductors by the incorporation of oxygen in the layer which helps to improve the HTM conductivity.[24] It has also been demonstrated that LiTFSI and *t*BP in organic HTMs can

Table 2 HOMO level and work function of the Th-PDI measured by different methods (local vacuum level = 0 eV)

Method	Sample	HOMO (eV)	WF (eV)
Electrochem.	Undoped	5.7	—
	Doped	—	—
KP	Undoped	—	5.0
	Doped	—	5.2
UPS[a]	Undoped	6.1	4.9
	Doped	6.3	5.3

[a] The normal thickness HTM as used in a cell could not be measured by UPS due to charging and a very thin film was used in this case.

Table 1 Summary of the photophysical and electrochemical properties of Th-PDI HTM

λ_{max} in solution[a] (nm)		λ_{max} in thin film[b] (nm)						HOMO–LUMO gap	
Abs	Emi	Abs	Emi	E^{ox}_{onset} (V)	E^{red}_{onset} (V)	E_{HOMO} (eV)	E_{LUMO} (eV)	Optical[c]	Ele. chem.[d]
585	695	585	711	1.00	−0.82	5.7	3.9	1.8	1.8

[a] UV-Vis absorption and fluorescence spectra were measured in chloroform solution. [b] Solid-state absorption and fluorescence spectra were measured by spin-coated thin-film. [c] Optical band-gap was calculated from the absorption threshold of the absorption spectrum. [d] Energy difference between the HOMO and LUMO, which was measured from cyclic voltammetry. Oxidation and reduction potentials are given in V *vs.* Ag/AgCl. E_{HOMO} and E_{LUMO} are given on the solid state scale (with the local vacuum level = 0 eV).

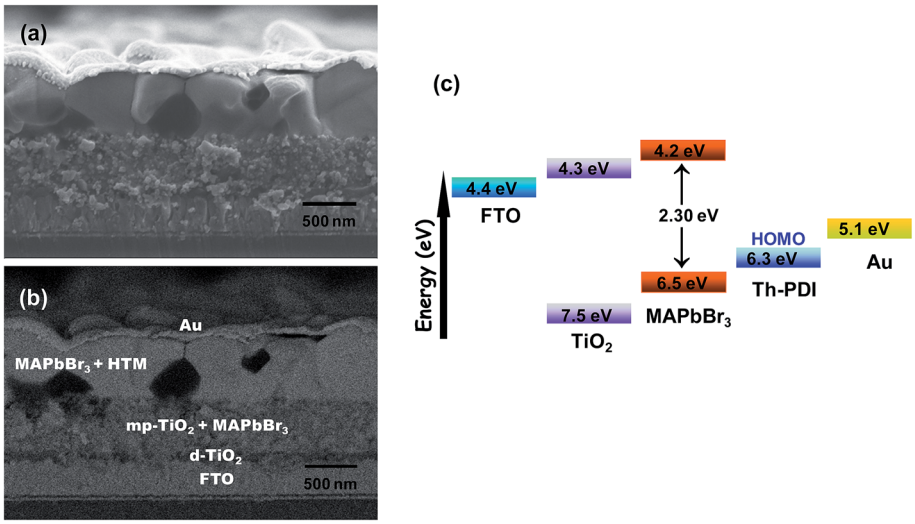

Fig. 2 Cross-sectional SEM image of a full mp-TiO_2 based device with (a) secondary (top) and (b) backscattered (bottom) electron detectors. (c) Schematic energy level alignment diagram of the cell. The HOMO value of the HTM given here is for the doped sample of Th-PDI, obtained by UPS. It should be noted that, when various energy levels are brought into contact with each other, some of the values may change.

suppress the interface charge carrier recombination[25] and this may also be a factor in the cell improvement after doping. Most of these cells show little if any hysteresis (this aspect will be discussed separately later).

Importantly, the reproducibility of these cells was very good: 24 cells were made on four separate batches (6 cells per batch); see Table ST1 and Fig. S5.† In all further cells discussed here, the doped HTM was used.

When the mp-TiO_2 was replaced by mp-Al_2O_3, (cell structure of FTO/d-TiO_2/mp-Al_2O_3/perovskite/HTM/Au), the device generated 180 mV higher photovoltage than with the mp-TiO_2 (V_{OC} from 1.23 to 1.41 V). However, the overall efficiency of the cell was reduced to 2.2% from 5.6%, mainly due to a large reduction in J_{SC}. It should be noted that these two types of cell architecture (with mp-TiO_2 *vs.* mp-Al_2O_3) do not just differ in the type of oxide that is being used to form the mesostructure, but also in the mechanism of photovoltaic action. In the cell with Al_2O_3 used as mesoporous layer, the photogenerated electrons are not injected into the mp-Al_2O_3 due to its very high-lying E_C edge: here the alumina merely acts as an inert scaffold onto which the perovskite is infiltrated when spin-coated. Therefore electron transport occurs through the perovskite itself to the front contact. The holes are injected to the organic HTM and flow through the HTM to the back electrode in both cases. In other words, while the mp-TiO_2 cell is a sensitized cell where both charges can be extracted within a relatively short distance from the locus of their generation, this is true only for the holes in the mp-Al_2O_3 cell; the electrons have to travel considerably larger distances on average in the perovskite to reach the front contact. This picture is somewhat simplistic because of the perovskite capping layer on the mp-substrate and the heterogeneity of the structure, meaning some holes also

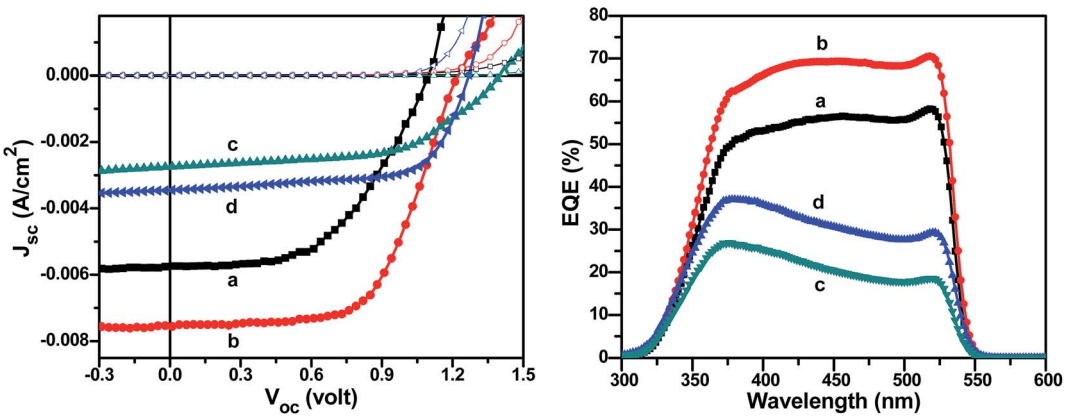

Fig. 3 (A) Photocurrent density *vs.* voltage curves of the different $MAPbBr_3$ cells: (a) FTO/d-TiO_2/mp-TiO_2/perovskite/undoped HTM/Au, (b) FTO/d-TiO_2/mp-TiO_2/perovskite/doped HTM/Au, (c) FTO/d-TiO_2/mp-Al_2O_3/perovskite/doped HTM/Au, and (d) FTO/d-TiO_2/perovskite/doped HTM/Au. Solid line with solid symbol: *J*–*V* under 1 sun illumination and solid line with hollow symbol: dark curves. (B) The external quantum efficiencies (EQE) of the corresponding devices.

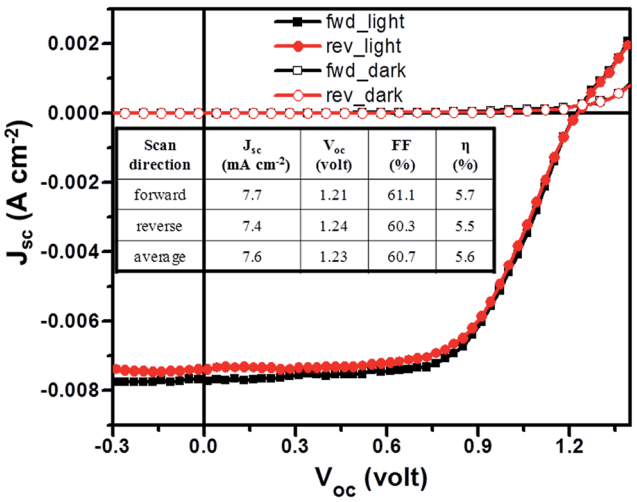

Scan direction	J_{sc} (mA cm^{-2})	V_{oc} (volt)	FF (%)	η (%)
forward	7.7	1.21	61.1	5.7
reverse	7.4	1.24	60.3	5.5
average	7.6	1.23	60.7	5.6

Fig. 4 Photocurrent density–voltage curves of a mp-TiO_2/$MAPbBr_3$/Th-PDI cell measured in both sweep directions. Scan rate 120 mV s^{-1}. Inset: the photovoltaic-parameters of the cell.

have to travel through this capping layer. However, since the concentration of electrons in the capping layer is low, electron–hole recombination in this layer will also be low, resulting in a relatively large hole diffusion length.

We also carried out experiments on planar cells. In the planar cell, both electrons and holes have to move distances that are considerably larger (on average) than those in the mp TiO_2 cell and furthermore, they do so in a region where both charge carriers exist. As seen in Table 3, the overall performance of the planar cells is somewhat better than that of the alumina cells. The main differences between the planar and alumina cells are the higher FF and lower V_{OC} of the planar cell. The lower V_{OC} is likely due to the greater contact between the perovskite and the TiO_2 since this contact may reduce the V_{OC} due to the conduction band misalignment. While most of the output parameters of the various cells are reasonably reproducible (see Tables T2 and T3 in ESI† for such data on alumina and planar cells), an exception was the FF of the planar cell, which varied more significantly. The photovoltaic parameters of the three best devices of different types are summarized in Table 3.

As the HTM used in this report absorbs light in the UV-Vis region (with $\lambda_{max} = 598$ nm and onset at ~700 nm) of the solar spectrum, the question arises whether or not the HTM contributes to the photocurrent generation. In order to check this, the external quantum efficiency (EQE) of all three different solar cell architectures was measured as well as that of the undoped HTM for the mp-TiO_2 cell, and the results are shown in Fig. 3B. In all cases no significant response was observed in the region where the HTM absorbs and the perovskite does not (between 550 nm and 700 nm) showing that the HTM does not contribute to the photo-generated current. Since the light passes through the perovskite before being absorbed by the HTM (either completely so for the planar cell or almost entirely, for the mesostructured cells), this does not lead to an appreciable loss in the cell. It would constitute a loss if the cell were used as a top cell in a tandem cell (the main reason why we study the bromide perovskite) but in this case, it is probable that the cell geometry and thickness of the HTM could be adjusted to minimize such a loss.

Comparing the EQE values with the *I–V* characteristics under one sun illumination (Fig. 3), there is reasonable correlation between the two sets of measurements (white light bias does not strongly affect the EQE measurements but small non-linearities of the light intensity *vs.* photocurrent may explain any minor discrepancies between the two measurements).

It is well-known that perovskite solar cells often exhibit hysteresis of the *I–V* characteristics. Different explanations for the hysteresis have been given in the literature,[26–29] but there is still no consensus. In general, it is at present thought to be connected to a build-up of charge, probably at the perovskite interfaces with the HTM and ETM, with ionic motion, filling/emptying of defects, or both involved. The photocurrent density–voltage (*J–V*) curves with both forward and reverse bias scans of a mp-TiO_2/$MAPbBr_3$/Th-PDI cell are shown in Fig. 4. There is only a *very small hysteresis* of the *J–V* characteristics. The values of the photovoltaic parameters in both scanning direction are given in the inset. We note that, in contrast to what is normally observed in the literature, the forward scan gives overall better performance than the reverse scan, although, as already noted, the difference is very small.

The equivalent planar cells exhibit a comparable degree of hysteresis (see Fig. S6†), while the cell on mp-Al_2O_3 shows an apparently somewhat larger (although unusual shape) hysteresis (Fig. S7†). Since, for the latter, some parameters improve and others become worse with sweep direction, the overall efficiency does not change much with sweep direction.

We compared the photovoltaic performance of the Th-PDI/$MAPbBr_3$ solar cell to that of $MAPbBr_3$ cells using two other HTMs *viz.* 2,2′,7,7′-tetrakis(*N*,*N*′-di-*p*-methoxyphenylamine)-9,9′-spirobifluorene (spiro-OMeTAD) and CBP. The cell configuration was FTO/d-TiO_2/mp-TiO_2/perovskite/HTM/Au. The device performances are summarized in Table 4. Th-PDI exhibits the best device performance in terms of efficiency of the cell under 1 sun illumination. It should be noted that the

Table 3 Summary of the cell performance with different device structures

Device structure	J_{SC} (mA cm^{-2})	V_{OC} (volt)	FF (%)	η (%)
FTO/d-TiO_2/mp-TiO_2/$MAPbBr_3$/Th-PDI/Au	7.6	1.23	60.7	5.6
FTO/d-TiO_2/mp-Al_2O_3/$MAPbBr_3$/Th-PDI/Au	2.7	1.41	56.2	2.2
FTO/d-TiO_2/$MAPbBr_3$/Th-PDI/Au	3.5	1.27	66.6	2.9

Table 4 Cell performance (best cells, average values between forward and reverse scans) with various HTMs. All devices were made on mp-TiO_2 substrates

Device structure	J_{SC} (mA cm^{-2})	V_{OC} (volt)	FF (%)	PCE (%)
$MAPbBr_3$/spiro-OMeTAD/Au	4.9	0.78	66.9	2.6
$MAPbBr_3$/CBP/Au	3.6	1.24	54.3	2.4
$MAPbBr_3$/Th-PDI/Au	7.6	1.23	60.7	5.6

devices based on Th-PDI and CBP as HTM produce a very similar V_{OC}, whereas spiro-OMeTAD results in a much lower V_{OC}, in agreement with the trends in the HOMO energy level of these HTMs (spiro-OMeTAD = −5.22 eV),[30] CBP = −6.23 eV,[31] and Th-PDI = −6.1 eV (undoped)/−6.3 eV (doped), as measured by UPS.

It is worth noting that refs. 13 and 15 both reported very high values of FF of ~0.8. Both these references used the same HTM (PIF8-TAA) which suggests a connection between these unusually high values of FF and this particular HTM.

We also compared the hysteresis of these cells with that of cells made with the two other HTMs. Some results are shown in Fig. S8† using spiro-OMeTAD and CBP as HTM. In brief, for spiro-OMeTAD as HTM, the results are comparable to the Th-PDI HTM: almost no hysteresis for the mp-TiO_2 cell, while hysteresis for the mp-Al_2O_3 cell is low but appreciable (6% change in efficiency dependent on scan direction). Using CBP as HTM, the hysteresis is very different with nearly 20% efficiency difference between the two scan directions (with the high values with forward scans) on mp-TiO_2. For mp-Al_2O_3-based cells there is almost no difference in apparent efficiency, although in this case there is a large hysteresis which, as for the same cells using Th-PDI, has individual parameters that nearly cancel out (see Fig. S8d†). While the behavior of the CBP-based cells is clearly unusual, the purpose of these experiments is to highlight the known important role of the charge-selective layers on the hysteresis behavior. This role may well be related to the degree of buildup of charge at the perovskite/HTM interface.

We carried out a preliminary ageing experiment to test the stability of the mp-TiO_2 devices. The (un-encapsulated) cell was stored in air (25–30% relative humidity) in the dark at room temperature. Fig. 5 shows the effect of this storage on the cell parameters. J_{SC} decreased monotonically over the test time period. Both the V_{OC} and the fill factor increased to a small but appreciable extent, which somewhat offset the drop in J_{SC}, resulting in an overall decrease in efficiency from 5.6% to 4.5% (nearly 20%) after 37 days. While we do not understand the cause(s) of these changes at present, the increase in fill factor

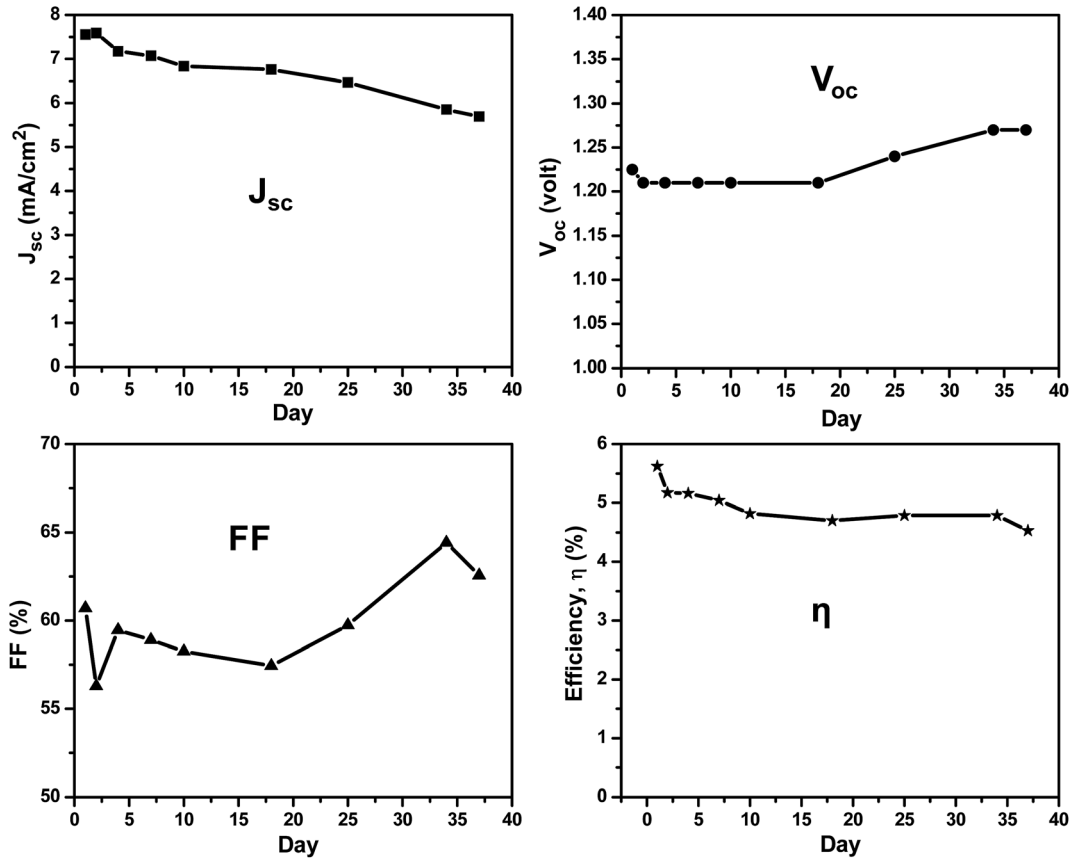

Fig. 5 Stability test of an unencapsulated mp-TiO_2 device stored in air (25–30% controlled relative humidity) and in the dark at room temperature using 1 sun illumination during the test periods.

and in V_{OC} is particularly interesting as an understanding of these increases might lead to improvements in the cell performance. There is almost no information in the literature on the stability of the bromide perovskite. The one exception is for a HTM-free cell that dropped ~80% in efficiency when kept 25 days at ambient conditions.[32]

Conclusions

We synthesized a small molecule with a PDI-core that was used as HTM to fabricate hybrid perovskite solar cells based on $MAPbBr_3$. On the basis of its UV-Vis spectrum, cyclic voltammetry and UPS measurements, the HOMO and LUMO levels of this molecule were determined. Three different solar cell architectures (mp-TiO_2, mp-Al_2O_3 and planar on dense TiO_2) were tested, based on $CH_3NH_3PbBr_3$ as light absorber. The architecture with mp-TiO_2 gave the best overall efficiency of 5.6% efficiency at a V_{OC} of 1.23 V with excellent reproducibility. The highest V_{OC} (1.41 V) was obtained, as expected from the mp-Al_2O_3 architecture, but exhibiting lower (2.2%) efficiency. The cells (except, to a small extent, the mp-Al_2O_3 ones) did not show any significant hysteresis with scan direction, possibly due to efficient charge transfer at the titania/perovskite and perovskite/HTM interfaces. We have also shown that the un-encapsulated cells are reasonably stable *ex situ*; the reduction in efficiency after storage in air at 25–30% relative humidity for 37 days was <20%. Further improvements should be feasible by improving the surface coverage of the perovskite and by optimizing the different layers in the device.

Experimental details

Full experimental details are given in the ESI.† In brief, a 40 wt% solution of methyl ammonium lead bromide ($MAPbBr_3$) perovskite solution was prepared by dissolving methyl ammonium bromide (MABr) and lead chloride ($PbCl_2$) in 3 : 1 molar ratio in anhydrous dimethyl formamide (DMF). The solution was then spin-coated onto the different substrates used in this work. The resulting films were heated on a hot plate at the desired temperature. The HTM was then deposited on the perovskite by spin-coating and finally gold was thermally evaporated through a rectangular shadow mask of area 0.24 cm^2. *J–V* curves were obtained with a Keithley 2400-LV SourceMeter under simulated AM1.5 sunlight, which was calibrated with a reference Si photodiode (IXOLAR™ High Efficiency SolarBIT, IXYS KXOB22-12X1L). The devices were measured through a 0.16 cm^2 mask and at a scan rate of 120 mV s^{-1} in both forward ($J_{SC} \rightarrow V_{OC}$) and reverse ($V_{OC} \rightarrow J_{SC}$) directions.

Conflict of interest

The authors declare no competing financial interest.

Acknowledgements

JD and RBKS thank the Planning and Budgeting Committee (PBC), Israel for postdoctoral fellowships. We thank Dr Tatyana Bendikov and Dr Thomas M. Brenner for the UPS and KP measurements respectively. This research was supported by the Leona M. and Harry B. Helmsley Charitable Trust, the Sidney E. Frank Foundation through the Israel Science Foundation, the Israel Ministry of Science, and the Israel National Nano-Initiative. DC holds the Sylvia and Rowland Schaefer Chair in Energy Research.

References

1 M. M. Lee, J. Teuscher, T. Miyasaka, T. N. Murakami and H. J. Snaith, *Science*, 2012, **338**, 643–647.
2 M. Liu, M. B. Johnston and H. J. Snaith, *Nature*, 2013, **501**, 395–398.
3 H.-S. Kim, S. H. Im and N.-G. Park, *J. Phys. Chem. C*, 2014, **118**, 5615–5625.
4 S. Kazim, M. K. Nazeeruddin, M. Grätzel and S. Ahmad, *Angew. Chem., Int. Ed.*, 2014, **53**, 2812–2824.
5 G. Hodes, *Science*, 2013, **342**, 317–318.
6 G. Hodes and D. Cahen, *Nat. Photonics*, 2014, **8**, 87–88.
7 C. Wehrenfennig, G. E. Eperon, M. B. Johnston, H. J. Snaith and L. M. Herz, *Adv. Mater.*, 2014, **26**, 1584–1589.
8 S. D. Stranks, G. E. Eperon, G. Grancini, C. Menelaou, M. J. P. Alcocer, T. Leijtens, L. M. Herz, A. Petrozza and H. J. Snaith, *Science*, 2013, **342**, 341–344.
9 A. Ishii, A. K. Jena and T. Miyasaka, *APL Mater.*, 2014, **2**, 091102.
10 E. Edri, S. Kirmayer, M. Kulbak, G. Hodes and D. Cahen, *J. Phys. Chem. Lett.*, 2014, **5**, 429–433.
11 J. Luo, J.-H. Im, M. T. Mayer, M. Schreier, M. K. Nazeeruddin, N.-G. Park, S. D. Tilley, H. J. Fan and M. Grätzel, *Science*, 2014, **345**, 1593–1596.
12 E. Edri, S. Kirmayer, D. Cahen and G. Hodes, *J. Phys. Chem. Lett.*, 2013, **4**, 897–902.
13 S. Ryu, J. H. Noh, N. J. Jeon, Y. C. Kim, W. S. Yang, J. Seo and S. I. Seok, *Energy Environ. Sci.*, 2014, **7**, 2614–2618.
14 Y. Tidhar, E. Edri, H. Weissman, D. Zohar, G. Hodes, D. Cahen, B. Rybtchinski and S. Kirmayer, *J. Am. Chem. Soc.*, 2014, **136**, 13249–13256.
15 J. H. Heo, D. H. Song and S. H. Im, *Adv. Mater.*, 2014, **26**, 8179–8183.
16 R. Sheng, A. Ho-Baillie, S. Huang, S. Chen, X. Wen, X. Hao and M. A. Green, *J. Phys. Chem. C*, 2015, **119**, 3545–3549.
17 M. C. R. Delgado, E.-G. Kim, D. A. da Silva Filho and J.-L. Bredas, *J. Am. Chem. Soc.*, 2010, **132**, 3375–3387.
18 R. R. Reghu, H. K. Bisoyi, J. V. Grazulevicius, P. Anjukandi, V. Gaidelis and V. Jankauskas, *J. Mater. Chem.*, 2011, **21**, 7811–7819.
19 X. Zhan, Z. A. Tan, B. Domercq, Z. An, X. Zhang, S. Barlow, Y. Li, D. Zhu, B. Kippelen and S. R. Marder, *J. Am. Chem. Soc.*, 2007, **129**, 7246–7247.
20 R. B. Kanth Siram, J. Smith, T. D. Anthopoulos and S. Patil, *J. Mater. Chem.*, 2012, **22**, 4450–4458.
21 M. Wiatrowski, E. Dobruchowska, W. Maniukiewicz, U. Pietsch, J. Kowalski, Z. Szamel and J. Ulanski, *Thin Solid Films*, 2010, **518**, 2266–2270.

22 Z. Li, J. Pei, Y. Li, B. Xu, M. Deng, Z. Liu, H. Li, H. Lu, Q. Li and W. Tian, *J. Phys. Chem. C*, 2010, **114**, 18270–18278.
23 Z. Li, Q. Dong, Y. Li, B. Xu, M. Deng, J. Pei, J. Zhang, F. Chen, S. Wen, Y. Gao and W. Tian, *J. Mater. Chem.*, 2011, **21**, 2159–2168.
24 A. Abate, T. Leijtens, S. Pathak, J. Teuscher, R. Avolio, M. E. Errico, J. Kirkpatrik, J. M. Ball, P. Docampo, I. McPherson and H. J. Snaith, *Phys. Chem. Chem. Phys.*, 2013, **15**, 2572–2579.
25 J. Krüger, R. Plass, L. Cevey, M. Piccirelli, M. Grätzel and U. Bach, *Appl. Phys. Lett.*, 2001, **79**, 2085–2087.
26 H. J. Snaith, A. Abate, J. M. Ball, G. E. Eperon, T. Leijtens, N. K. Noel, S. D. Stranks, J. T.-W. Wang, K. Wojciechowski and W. Zhang, *J. Phys. Chem. Lett.*, 2014, **5**, 1511–1515.
27 H.-W. Chen, N. Sakai, M. Ikegami and T. Miyasaka, *J. Phys. Chem. Lett.*, 2015, 164–169.
28 A. K. Jena, H.-W. Chen, A. Kogo, Y. Sanehira, M. Ikegami and T. Miyasaka, *ACS Appl. Mater. Interfaces*, 2015, **7**, 9817–9823.
29 W. Tress, N. Marinova, T. Moehl, S. M. Zakeeruddin, M. K. Nazeeruddin and M. Grätzel, *Energy Environ. Sci.*, 2015, **8**, 995–1004.
30 H. Choi, S. Park, S. Paek, P. Ekanayake, M. K. Nazeeruddin and J. Ko, *J. Mater. Chem. A*, 2014, **2**, 19136–19140.
31 M. Kröger, S. Hamwi, J. Meyer, T. Riedl, W. Kowalsky and A. Kahn, *Org. Electron.*, 2009, **10**, 932–938.
32 S. Aharon, B. E. Cohen and L. Etgar, *J. Phys. Chem. C*, 2014, **118**, 17160–17165.